Decision Tree 2 provides an approach for setting specifications for polymorphs in the drug substance when at least one form is known to have low solubility based on the BCS. If relevant and adequate specifications for polymorphs are included in the USP, ANDA applicants may adopt these specifications for the drug substance polymorphic form. Otherwise, we recommend that a new specification for the drug substance polymorphic form be established.
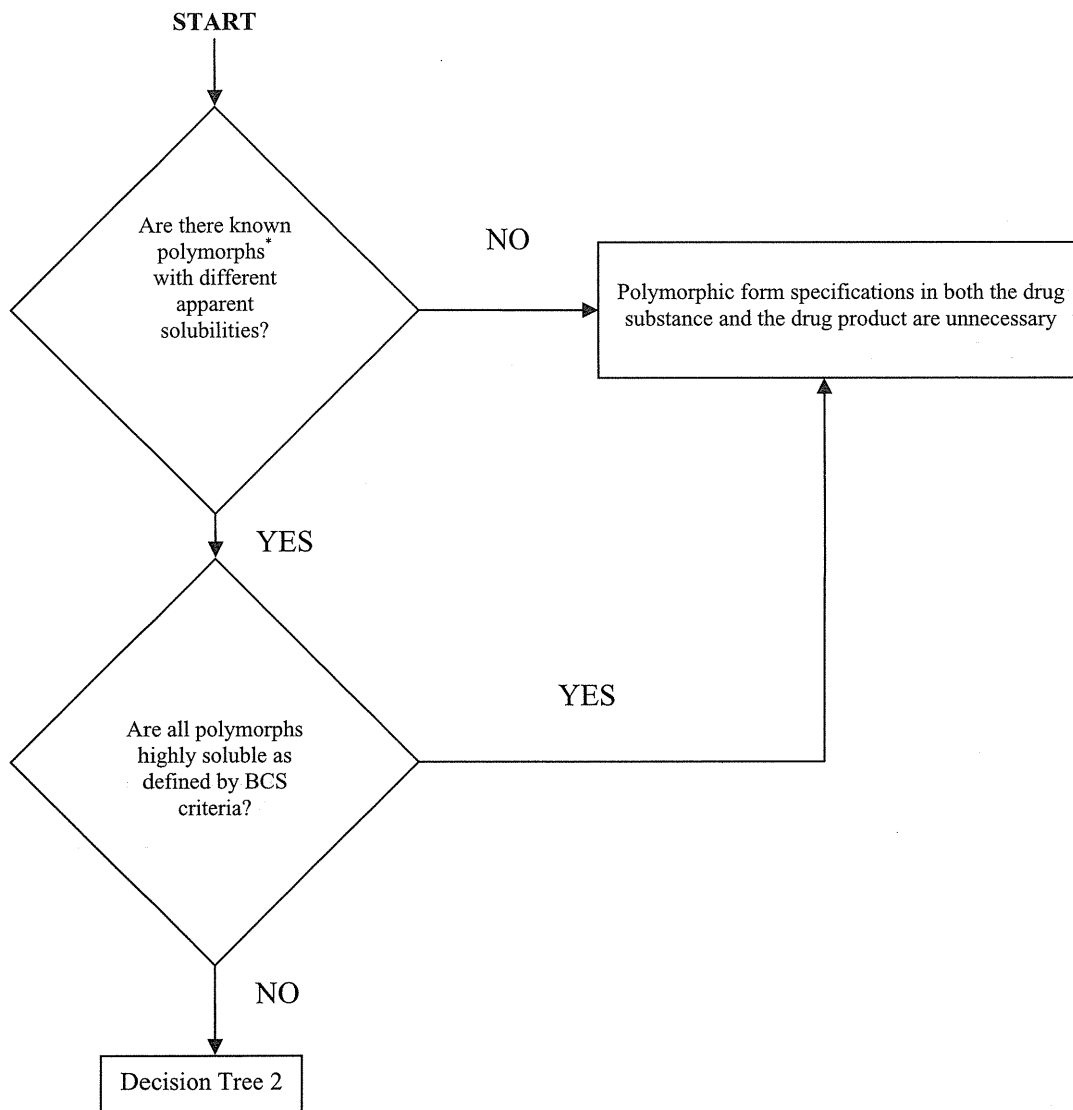
C. Investigating the Importance of Setting Specifications for Polymorphs in Drug Products

Decision Tree 3 provides an approach when considering whether to set specifications for polymorphs in the drug product. Generally, specifications for polymorphs in drug products are not necessary if the most thermodynamically stable polymorphic form is used or if the same form is used in an approved product of the same dosage form. However, since manufacturing processes can affect the polymorphic form, we recommend that you use caution if a metastable form is used.

Drug product performance testing (e.g., dissolution testing) can also generally provide adequate control of polymorph ratio changes that can influence drug product BA/BE for poorly soluble drugs. In such instances, setting specifications for polymorphs in the drug product would generally not be considered important for ensuring adequate product performance. Only in rare cases would we recommend setting specifications for polymorphic forms in drug products.
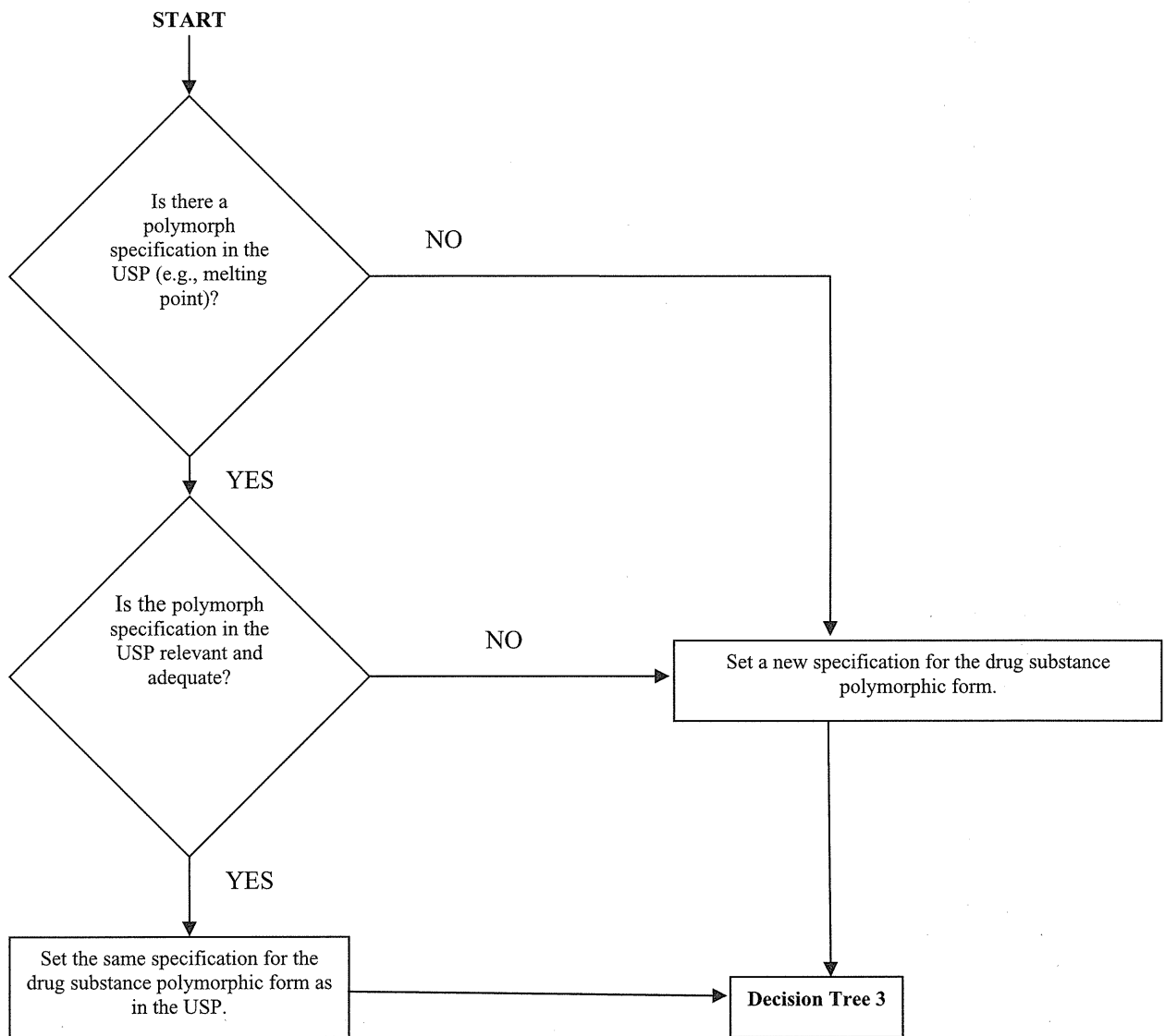

ATTACHMENT 1 – DECISION TREE 1

Decision Tree 1   Investigating whether to set specifications for polymorphs for solid oral and suspension dosage form products.

START

Are there known polymorphs* with different apparent solubilities?

NO

Polymorphic form specifications in both the drug substance and the drug product are unnecessary

YES

Are all polymorphs highly soluble as defined by BCS criteria?

YES

NO

Decision Tree 2

*We recommend that you consider only those polymorphs that are likely to form during manufacture of the drug substance, manufacture of the drug product, or while the drug substance or drug product is in storage. See footnote 7 in this guidance document.
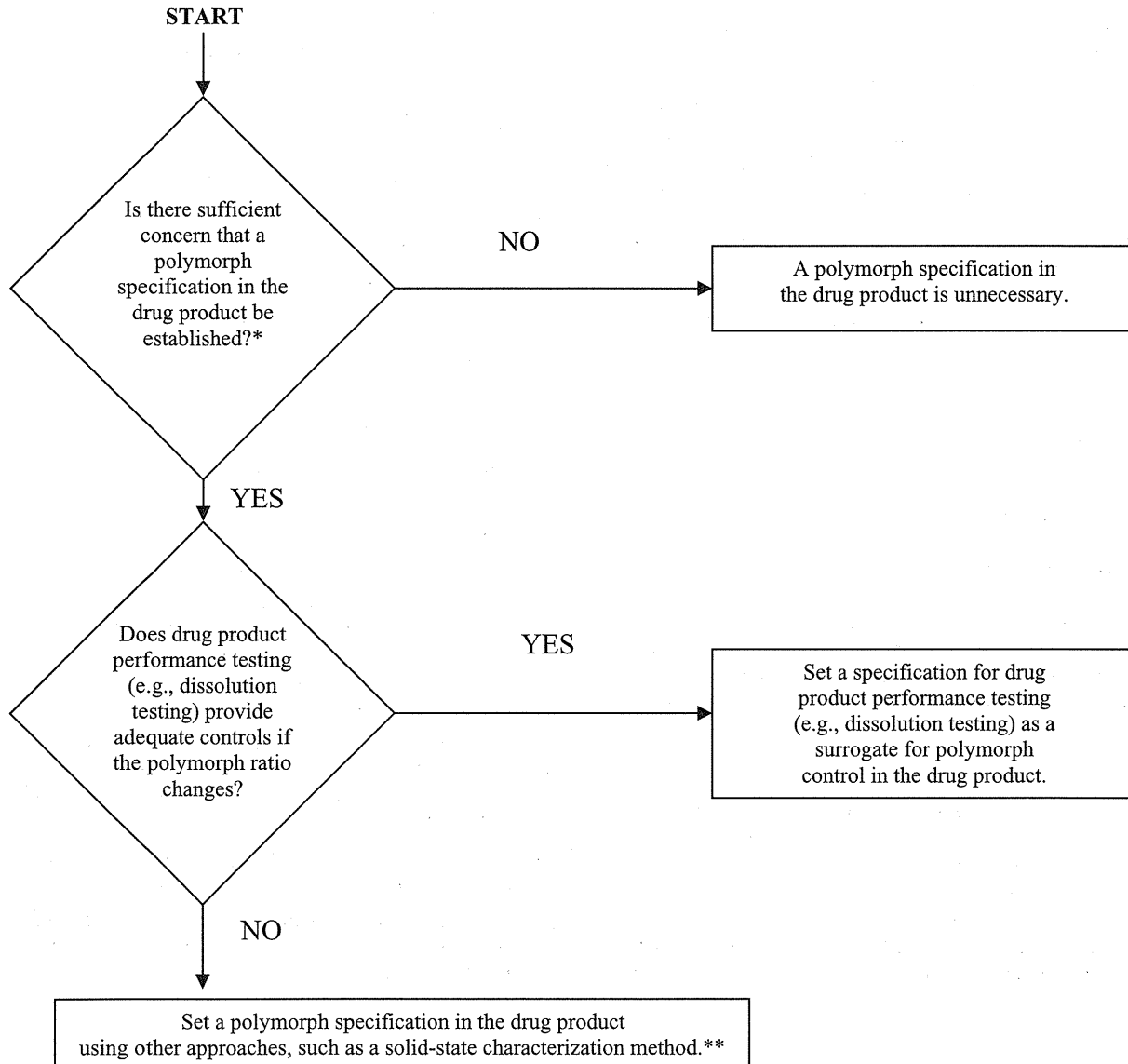
8

ATTACHMENT 2 – DECISION TREE 2

Decision Tree 2   Setting specifications for polymorphs in drug substances for solid oral and suspension dosage form products.

START

Is there a polymorph specification in the USP (e.g., melting point)?

NO

YES

Is the polymorph specification in the USP relevant and adequate?

NO

Set a new specification for the drug substance polymorphic form.

YES

Set the same specification for the drug substance polymorphic form as in the USP.

Decision Tree 3

9

ATTACHMENT 3 – DECISION TREE 3

Decision Tree 3   Investigating whether to set specifications for polymorphs in drug products for solid oral and suspension dosage form products.

START

```
                    Is there sufficient
                    concern that a
                    polymorph              NO
                    specification in the  ───────────►  A polymorph specification in
                    drug product be                     the drug product is unnecessary.
                    established?*

                           │ YES
                           ▼
                    Does drug product
                    performance testing
                    (e.g., dissolution     YES         Set a specification for drug
                    testing) provide      ───────────► product performance testing
                    adequate controls if               (e.g., dissolution testing) as a
                    the polymorph ratio                surrogate for polymorph
                    changes?                           control in the drug product.

                           │ NO
                           ▼
                Set a polymorph specification in the drug product
           using other approaches, such as a solid-state characterization method.**
```

*In general, there may not be a concern if the most thermodynamically stable polymorphic form is used or the same form is used in a previously approved product of the same dosage form.

**Drug product performance testing (e.g., dissolution testing) can generally provide adequate control of polymorph ratio changes for poorly soluble drugs, which may influence drug product BA/BE. Only in rare cases would polymorphic form characterization in the drug product be recommended.

10

別添資料2

01/2005:50900

5.9. POLYMORPHISM

Polymorphism (or crystal polymorphism) is a phenomenon related to the solid state; it is the ability of a compound in the solid state to exist in different crystalline forms having the same chemical composition. Substances that exist in a non-crystalline solid state are said to be amorphous.

When this phenomenon is observed for a chemical element (for example, sulphur), the term allotropy is used instead of polymorphism.

The term pseudopolymorphism is used to describe solvates (including hydrates), where a solvent is present in the crystal matrix in stoichiometric proportions; the term may also be extended to include compounds where the solvent is trapped in the matrix in variable proportions. However the term pseudopolymorphism is ambiguous because of its use in different circumstances. It is therefore preferable to use only the terms "solvates" and "hydrates".

Where a monograph indicates that a substance shows polymorphism, this may be true crystal polymorphism, occurence of solvates, allotropy or occurrence of the amorphous form.

The identity of chemical composition implies that all crystalline and amorphous forms of a given species have the same chemical behaviour in solution or as a melt; in contrast, their physico-chemical and physical characteristics (solubility, hardness, compressibility, density, melting point, etc.), and therefore their reactivity and bioavailability may be different at the solid state.

When a compound shows polymorphism, the form for which the free enthalpy is lowest at a given temperature and pressure is the most thermodynamically stable. The other forms are said to be in a metastable state. At normal temperature and pressure, a metastable form may remain unchanged or may change to a thermodynamically more stable form.

If there are several crystalline forms, one form is thermodynamically more stable at a given temperature and pressure. A given crystalline form may constitute a phase that can reach equilibrium with other solid phases and with the liquid and gas phases.

If each crystalline form is the more stable within a given temperature range, the change from one form to another is reversible and is said to be enantiotropic. The change from one phase to another is a univariate equilibrium, so that at a given pressure this state is characterised by a transition temperature. However, if only one of the forms is stable over the entire temperature range, the change is irreversible or monotropic.

Different crystalline forms or solvates may be produced by varying the crystallisation conditions (temperature, pressure, solvent, concentration, rate of crystallisation, seeding of the crystallisation medium, presence and concentration of impurities, etc.).

The following techniques may be used to study polymorphism:

— X-ray diffraction of powders,

— X-ray diffraction of single crystals,

— thermal analysis (2.2.34) (differential scanning calorimetry, thermogravimetry, thermomicroscopy),

— microcalorimetry,

— moisture absorption analysis,

— optical and electronic microscopy,

— solid-state nuclear magnetic resonance,

— infrared absorption spectrophotometry (2.2.24),

— Raman spectrometry (2.2.48),

— measurement of solubility and intrinsic dissolution rate,

— density measurement.

These techniques are often complementary and it is indispensable to use several of them.

Pressure/temperature and energy/temperature diagrams based on analytical data are valuable tools for fully understanding the energetic relationship (enantiotropism, monotropism) and the thermodynamic stability of the individual modifications of a polymorphic compound.

For solvates, differential scanning calorimetry and thermogravimetry are preferable, combined with measurements of solubility, intrinsic dissolution rate and X-ray diffraction.

For hydrates, water sorption/desorption isotherms are determined to demonstrate the zones of relative stability.

In general, hydrates are less soluble in water than anhydrous forms, and likewise solvates are less soluble in their solvent than unsolvated forms.

5. General texts

別紙4

研究成果の刊行

書籍

著者氏名	論文タイトル名	書籍全体の編集者名	書　籍　名	出版社名	出版地	出版年	ページ

雑誌

発表者氏名	論文タイトル名	発表誌名	巻号	ページ	出版年
K. Kawakami, T. Harada, K. Miura, Y. Yoshihashi, E. Yonemochi, K. Terada, H. Moriyama	Relationship between crystallization tendencies during cooling from melt and isothermal storage: Toward a general understanding of physical stability of pharmaceutical glasses	Mol. Pharmaceutics			2014
Shibata H, Yomota C, Okuda H.	Simultaneous determination of polyethylene glycol-conjugated liposome components by using reversed-phase high-performance liquid chromatography with UV and evaporative light scattering detection.	AAPS PharmSciTech.	14	811-7	2013

Relationship between Crystallization Tendencies during Cooling from Melt and Isothermal Storage: Toward a General Understanding of Physical Stability of Pharmaceutical Glasses

Kohsaku Kawakami,*[,†] Takuji Harada,[†,‡] Keiko Miura,[§] Yasuo Yoshihashi,[||] Etsuo Yonemochi,[||,⊥] Katsuhide Terada,[||] and Hiroshi Moriyama[‡]

[†]Biomaterials Unit, International Center for Materials Nanoarchitectonics, National Institute for Materials Science, 1-1 Namiki, Tsukuba, Ibaraki 305-0044, Japan

[‡]Faculty of Science, Toho University, 2-2-1 Miyama, Funabashi, Chiba 274-8510, Japan

[§]Industrial Application Division, Japan Synchrotron Radiation Research Institute (JASRI/SPring8), 1-1-1 Kouto, Sayo, Hyogo 679-5198, Japan

[||]Faculty of Pharmaceutical Sciences, Toho University, 2-2-1 Miyama, Funabashi, Chiba 274-8510, Japan

ABSTRACT: The lack of protocols to predict the physical stability has been one of the most important issues in the use of amorphous solid dispersions. In this paper, the crystallization behaviors of pharmaceutical glasses, which have large variations in their crystallization tendencies, have been investigated. Although each compound appears to have a wide variation in their crystallization time, the initiation time for crystallization could be generalized as a function of only T_g/T, where T_g and T are the glass transition temperature and storage temperature, respectively. All compounds in which crystallization was mainly governed by temperature had similar activation energies for crystallization initiation, ca. 210−250 kJ/mol, indicating that physical stability at any temperature is predictable from only T_g. Increased stability is expected for other compounds, where crystallization is inhibited by an large energetic barrier, and stochastic nucleation plays an important role in initiating crystallization. The difference in the dominant factor, either temperature or pressure, appeared to correlate with the nucleation mechanism, and this could be determined by a cool−heat cycle after melting using thermal analysis. This conclusion should make prediction of physical stability of amorphous formulations easier, although the investigation was conducted under ideal conditions, which eliminated surface effects.

KEYWORDS: amorphous, crystallization, nucleation, glass transition temperature, activation energy, stability prediction
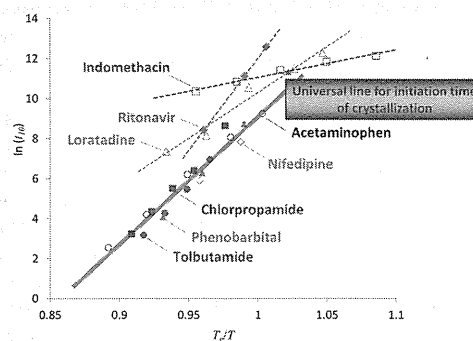
INTRODUCTION

Amorphous solid dispersion is one of the most important formulation technologies for poorly soluble drugs because it can improve the dissolution process and, therefore, their bioavailability.[1−4] However, although amorphization is regarded as a conventional technology for injectable formulations, the number of marketed oral amorphous formulations is still limited. One of the major concerns for the use of amorphous forms has been their physical stability.[3,4] In most cases, injectable formulations are under the control of medical personnel. However, oral formulations are usually handled by patients, and the stability requirements are more severe. In addition, amorphization technology is frequently applied to peptide drugs in the case of injectable formulations, of which the intrinsic crystallization tendency is very low. From the viewpoint of developmental studies, the lack of an accelerated study protocol for predicting the crystallization behavior of amorphous forms has been an issue that inhibits their wide use.[3−5]

Many attempts have been made to derive a general rule that determines the crystallization tendency of organic compounds. Requirements for chemical structures of good glass formers have been indicated, e.g., a large molecular weight with a low number of benzene rings, low level of molecular symmetry, many rotatable bonds, branched carbon skeletons, and electronegative atoms.[6−8] Also, good glass formers tend to have a large enthalpy/entropy of fusion, large free energy difference between crystalline and amorphous states, and high melting temperatures.[7] Interactions between the molecules and molecular mobility are also important factors.[9,10] Fragility,[11,12] which is a measure of the non-Arrhenius characteristics of liquids/glasses, is another factor that is thought to influence crystallization ability.[7,13] However, although these factors have been shown to correlate with the glass forming ability to some

A

Table 1. List of Model Drugs Used in This Study

classification[a]	compound	abbreviation	M_w	T_m (°C)[b]	T_g (°C)[c]	supplier
I	chlorpropamide	CPA	276.7	122	16	Sigma-Aldrich (St. Louis, USA)
	haloperidol	HPD	375.9	150	27[d]	Nacalai Tesque (Kyoto, Japan)
	tolbutamide	TLB	270.3	128	5	Wako Pure Chemicals (Osaka, Japan)
II	acetaminophen	AAP	151.2	169	24	MP Biomedicals (Santa Ana, USA)
	nifedipine	NDP	346.3	173	46	Alexis Biochemicals (San Diego, USA)
III	loratadine	LTD	382.9	135	38	Tokyo Chemical Industry (Tokyo, Japan)
	ritonavir	RTV	721.0	127	47	LKT Laboratories (St. Paul, USA)

[a]Classification system introduced by Taylor et al. (see text). [b]Peak temperature. [c]Onset temperature. [d]Determined by high-speed DSC.

extent, they do not provide quantitative information on the crystallization behavior of a specific compound. Representative examples of quantitative measures of glass-forming ability are the reduced glass transition temperature, which is a ratio of glass transition and melting temperatures, and onset cold crystallization temperature.[14] However, these investigations have mainly been made on metallic alloys, and there are few such observations for organic compounds. Ping et al. investigated the glass-forming ability of o-terphenyl and structurally related compounds and concluded that compounds with high reduced glass transition temperatures (above 0.73) were good glass formers, while those with low reduced glass transition temperatures (below 0.68) were poor glass formers.[15]

This knowledge has been developed mainly from observations of crystallization behavior during cooling from the melt. It does not provide direct information on the isothermal crystallization behavior, which is of great interest for formulators. Dynamics of molecules, which should have a great impact on the crystallization behavior, are influenced by both thermal energy (temperature) and molecular packing (pressure/volume).[16,17] Both factors are continuously changing and have a significant impact on the crystallization process during cooling, while basically, isothermal crystallization should rely on fluctuations in the local energy to break the energetic barrier of crystallization, although the free energy change accompanied by crystallization is essentially the same for both types of processes. Presented here is an observation of the isothermal crystallization behaviors of model compounds, which have various crystallization tendencies during cooling from the melt and subsequent reheating. The relationship between the crystallization behavior and their dominating factor, either temperature or pressure, is discussed. A simple prediction protocol for physical stability is also provided.

MATERIALS AND METHODS

Materials. All the model drugs used in this study are listed in Table 1 with their supplier, abbreviation, and basic characteristics. All compounds were used as supplied.

Differential Scanning Calorimetry (DSC). DSC measurements were performed on a DSC Q2000 (TA Instruments, New Castle, DE, USA), which were periodically calibrated using indium and sapphire. Dry nitrogen was used as the inert gas at a flow rate of 50 mL/min. Crimped aluminum pans were used for the measurements except in the case of nifedipine (NDP), for which hermetic aluminum pans were used, because sorption of a trace amount of moisture during handling dramatically influenced its crystallization. All evaluations were at least performed in triplicate. Heat capacity measurements were performed in the modulated DSC mode using the

protocol established previously[18] in which the sample (ca. 10 mg) was heated in a crimped T-zero aluminum pan at 2 °C/min with a 60 s period and 0.5 °C amplitude. Amorphous samples were prepared by quenching at 50 °C/min from above the melting temperature. Although accuracy of this cooling rate was not assured by the manufacturer of the instrument, it was confirmed to be successfully achieved according to the temperature data.

X-ray Powder Diffraction (XRPD). XRPD patterns were acquired on a Rigaku RINT Ultima X-ray diffraction system (Rigaku Denki, Tokyo, Japan) using Cu Kα radiation. The voltage and the current were 40 kV and 40 mA, respectively. Data were collected between 3° and 40° (2θ) at intervals of 0.02° with a scan speed of 2°/min.

Isothermal Annealing. After quenching in the DSC, all the glass samples were subjected to annealing at various temperatures. Annealing shorter than 48 h was performed in DSC. When longer annealing was required, the samples in the DSC pans were stored in desiccators with silica gel in temperature-controlled ovens. The difference in the storage protocol was negligible for all the compounds.

Synchrotron Wide-Angle X-ray Diffraction (WAXD). Simultaneous measurements of WAXD/DSC were performed at BL40B2 of the synchrotron facility SPring-8 (Sayo, Japan). The wavelength of the incident X-ray beam was 0.100 nm. A Hamamatsu flat panel (50um/pixel) was used as the 2D detector for WAXD measurements and the sample-to-detector distance was 53.9 mm, which was calibrated using silver behenate. The exposure time was 1 s. The WAXD image was displayed using LabView software ImageView92. Exothermic heat flow due to crystallization of tolbutamide (TLB) and acetaminophen (AAP) was observed with Thermo Plus DSC (Rigaku, Tokyo, Japan). TLB was melted at 140 °C, followed by cooling at 5 °C/min. AAP was melted at 200 °C, followed by cooling at 30 °C/min to 0 °C and reheating at 5 °C/min.

Thermal Stability of Model Compounds. The thermal stability of each drug was investigated using thermogravimetric (TG) analysis on SDT Q600 (TA Instruments, New Castle, DE, USA) and high-performance liquid chromatography (HPLC). TG analysis was performed up to the melting temperatures to observe weight loss due to decomposition and sublimation. The compounds that exhibited weight loss more than 0.01% in the TG study were subjected to HPLC analysis on a Shimadzu Prominence (Shimadzu, Kyoto, Japan) equipped with a Cosmosil 5C18-AR-II (150 mmL × 5.0 mmID, Nacalai Tesque, Kyoto, Japan) with a flow rate of 1 mL/min. The column was equilibrated by acetonitrile/water = 5/95, and measurements were done with this mobile phase for 10 min, followed by a gradual change to 100/0 over 40 min and
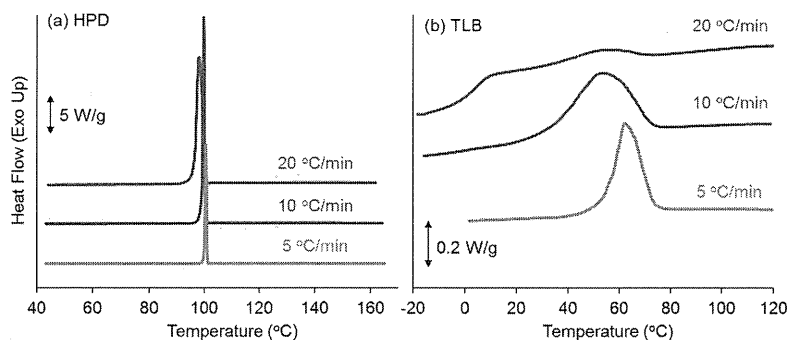
Figure 1. DSC cooling curves of the class I compounds from the melt.[17] The cooling rates are indicated.

161 elution by acetonitrile for 10 min. The detection wavelength
162 and injection volume were 210 nm and 2 μL, respectively.
163 Some compounds exhibited weight loss at very low temperature
164 (<100 °C), followed by flat baselines. In such cases, the weight
165 loss was interpreted as removal of adsorbed water, and only the
166 weight loss after the flat baseline was evaluated.

167 **The Classification System.** The basic idea ("protocol for
168 classification") for the classification system presented below was
169 introduced by Taylor et al.,[7] which was established by observing
170 the crystallization behavior during cooling from the melt and
171 subsequent reheating. Their purpose was classification of the
172 compounds on the basis of crystallization tendency during the
173 cooling and reheating, and the origin of different crystallization
174 behaviors was not discussed in detail. We have added our
175 interpretation of the dominant factor in the crystallization
176 process, that is, either temperature or pressure, based on the
177 investigation of the cooling rate-dependence of the crystal-
178 lization temperature, as described next.

179 Class I: Crystallization is dominated by thermodynamics.
180 Temperature (degree of supercooling) is a dominant factor for
181 controlling the crystallization process. Protocol for classifica-
182 tion: Compounds that crystallized during cooling from the
183 melt at 20 °C/min.

184 Class II: Crystallization is influenced by competition between
185 thermodynamic and kinetic factors. Basically temperature
186 dominates crystallization; however, the transformation is
187 disturbed by steric hindrance (local pressure).

188 Protocol for classification: Compounds that do not crystallize
189 during cooling from the melt at 20 °C/min but crystallize
190 during subsequent reheating at 20 °C/min.

191 Class III: Crystallization is dominated by pressure. Stochastic
192 nucleation plays a dominant role in controlling the crystal-
193 lization process.

194 Protocol for classification: Compounds that do not crystallize
195 during the cooling/reheating cycle presented above.

196 An amorphous state is thermodynamically unstable and
197 always seeks opportunities to transform into a crystalline state.
198 The initial nucleation step is a trigger for this transformation. If
199 the energetic barrier for nucleation is very small, basically due
200 to a small steric hindrance, crystallization should be controlled
201 by the free energy difference between the crystalline and
202 amorphous states, which can be described as a function of only
203 temperature under ambient pressure condition. This is a
204 situation where the system is thermodynamically (temperature)
205 controlled (class I). If the melt is cooled from the melting
206 temperature, crystallization should occur at the same temper-
207 ature regardless of the cooling rate in this case. Homogeneous
208 nucleation may be expected because no templates are required.

209 In contrast, the free energy difference is less important if the
210 energetic barrier for the nucleation is large enough. In this case
211 where probability of nucleation is very low, the transformation
212 relies on local thermal and density fluctuations to induce
213 "stochastic" nucleation. Once the nuclei are formed, crystal
214 growth should follow, using the nuclei as templates. This
215 "pressure-controlled" situation should be initiated by hetero-
216 geneous nucleation, and crystallization during cooling and
217 reheating is not likely to occur (class III). If there is a moderate
218 energetic barrier for nucleation, crystallization may occur
219 during the cooling and reheating cycle. The cooling rate
220 should have a significant impact on the crystallization
221 temperature because it influences the frustration in the
222 molecular structure that determines the energetic barrier for
223 nucleation (class I or II).

224 Figure 1 shows DSC cooling curves from the melt for
haloperidol (HPD) and TLB,[19] both of which are classified as
225 class I compounds. HPD always crystallized at 100 °C
226 regardless of the cooling rate. The crystallization of HPD is
227 clearly dominated by temperature, because if the kinetic factor
228 influenced the crystallization process, the crystallization
229 temperature should depend on the cooling rate. Such cooling
230 rate-insensitive crystallization can be found for many class I
231 compounds including atenolol, benzamide, caffeine, and
232 indoprofen.[7] TLB also crystallizes during the cooling scan;
233 however, the crystallization temperature depends on the
234 cooling rate. Moreover, only partial crystallization was observed
235 when TLB was cooled at 20 °C/min, and glass transition
236 behavior was also detected at 3 °C. Thus, crystallization of TLB
237 seemed to be dominated by temperature but there was also a
238 kinetic contribution. When TLB was cooled at 50 °C/min, it
239 failed to crystallize in the cooling process but crystallized in the
240 subsequent reheating. Thus, while both class I and II
241 compounds are mainly controlled by temperature, there is a
242 difference in the relative contribution of thermodynamic and
243 kinetic factors in the crystallization process. Theoretically, class
244 III compounds should crystallize as well if they are cooled or
245 reheated at a very slow scan rate, but this was found to be
246 practically impossible.

■ **RESULTS AND DISCUSSION**

Thermal Stability of Model Compounds. In the
249 following experiments, each drug was melted before assessment
250 of crystallization behavior and heat capacity measurement. If
251 decomposition occurs, it can influence the crystallization rate
252 significantly. All the compounds used in this study were
253 confirmed to be stable during the 1 min melting. Thus, the
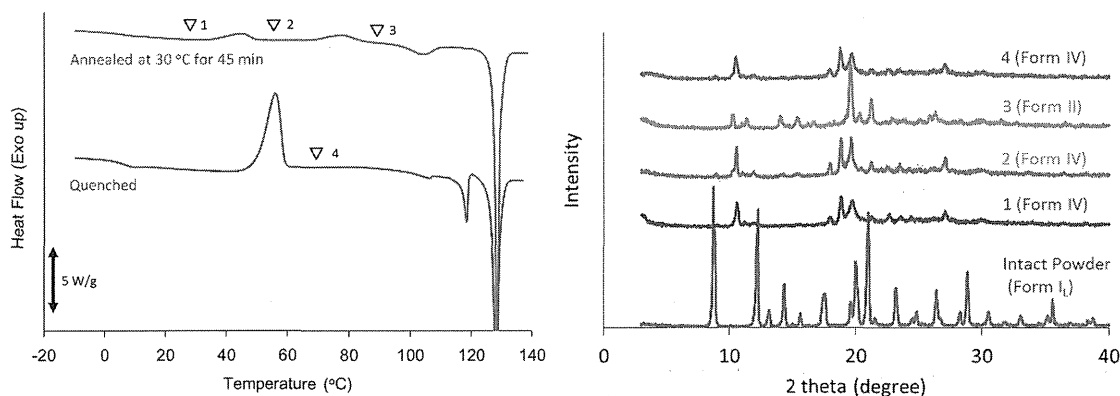254 melt—quench procedure did not seem to produce degradation

Figure 2. (left) DSC heating curves (10 °C/min) of quenched and annealed TLB. The quench was done in the DSC at a cooling rate of 50 °C/min. The annealing was also performed in the DSC at 30 °C for 45 min. The XRPD patterns of the samples at the indicated point (1–4) on the DSC curves are presented on the right with assignment of the crystal forms. (right) The XRPD patterns of the samples collected from the DSC pan. The DSC measurements were terminated at the indicated point in the left figure for supplying the samples to the XRPD analysis. The sample weight for this purpose was larger than 10 mg.
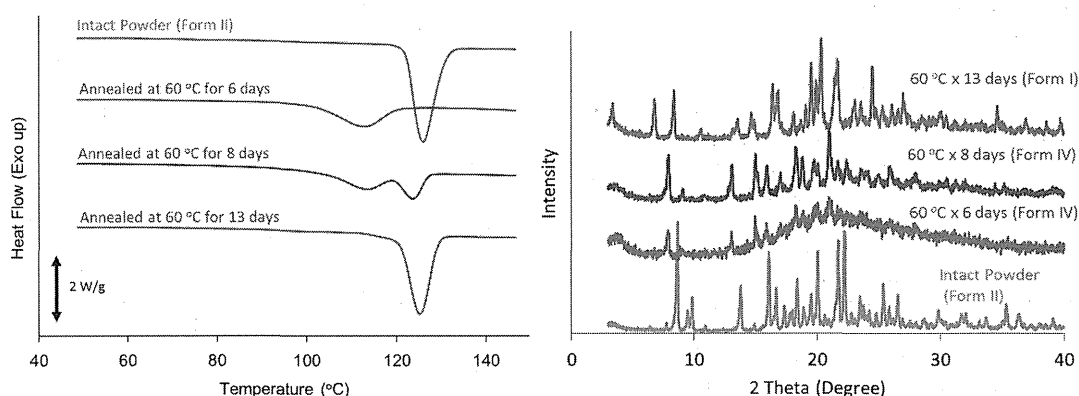
Figure 3. (left) DSC heating curves (10 °C/min) of annealed RTV after the quenching. The annealing was done at 60 °C in a temperature-controlled oven for the indicated period. (right) The XRPD patterns of the annealed RTV at 60 °C for the indicated period with assignment of the crystal forms.

products. Most of the compounds were also stable during the storage performed in this study. However, ritonavir (RTV) produced approximately 5% of degradation products during storage at 60 °C for 1 month. Although no degradation products were detected for loratadine (LTD) after 1 month of storage at 60 °C, the sample was slightly red in color, which obviously indicated degradation. However, crystallization of both RTV and LTD was almost completed in one month at 60 °C. This study focuses on the 10% crystallization time, which was completed in 3 days and 1 day for RTV and LTD, respectively, for which impact of degradation was negligible.

Determination of Crystallinity. The crystallinity of class I and II compounds was determined from the crystallization enthalpy observed during the heating process in DSC measurements, except for NDP. Figure 2 shows the DSC heating curves and XRPD patterns of TLB. The quenched TLB crystallized to form IV at ca. 50 °C in the heating process, revealed by the XRPD analysis and an exothermic enthalpy of ca. 72 J/g. During storage at 30 °C, the quenched TLB gradually crystallized to form IV. Figure 2 also shows the heating curve of TLB, which was stored at 30 °C for 45 min. It exhibited a small exothermic peak at ca. 40 °C, which was due to crystallization of the remaining amorphous part to form IV.

It transformed to form II at ca. 80 °C, and to form I_h (high-temperature stable form of form I) at ca. 100 °C. The crystallinity, X, of the stored sample can be calculated as follows.

$$X(\%) = 100\{\Delta H / (\Delta H_q - \int_T^{T_q} \Delta Cp)\} \tag{1}$$

where ΔH and ΔH_q are the crystallization enthalpies of the annealed and quenched (i.e., no annealing) samples, respectively. T and T_q are the crystallization temperatures, and peak temperatures were used for simplicity. ΔC_p is the heat capacity difference of the amorphous and crystalline forms obtained by temperature-modulation measurements. The integration term was calculated numerically. In a similar procedure, crystallinity of the recrystallized quenched sample was proved to be almost 100%. Form I_h melt temperature is at 127 °C with a melting enthalpy of ca. 106 J/g. Heat capacity difference between forms I and IV were negligible, and they exhibited lower values than that of supercooled liquid by ca. 0.45 J/g. Because the temperature difference between melting of form I_h and crystallization to form IV was approximately 77 °C, expected crystallization enthalpy of form IV is 71 J/g, which almost agrees with the observed value, 72 J/g.
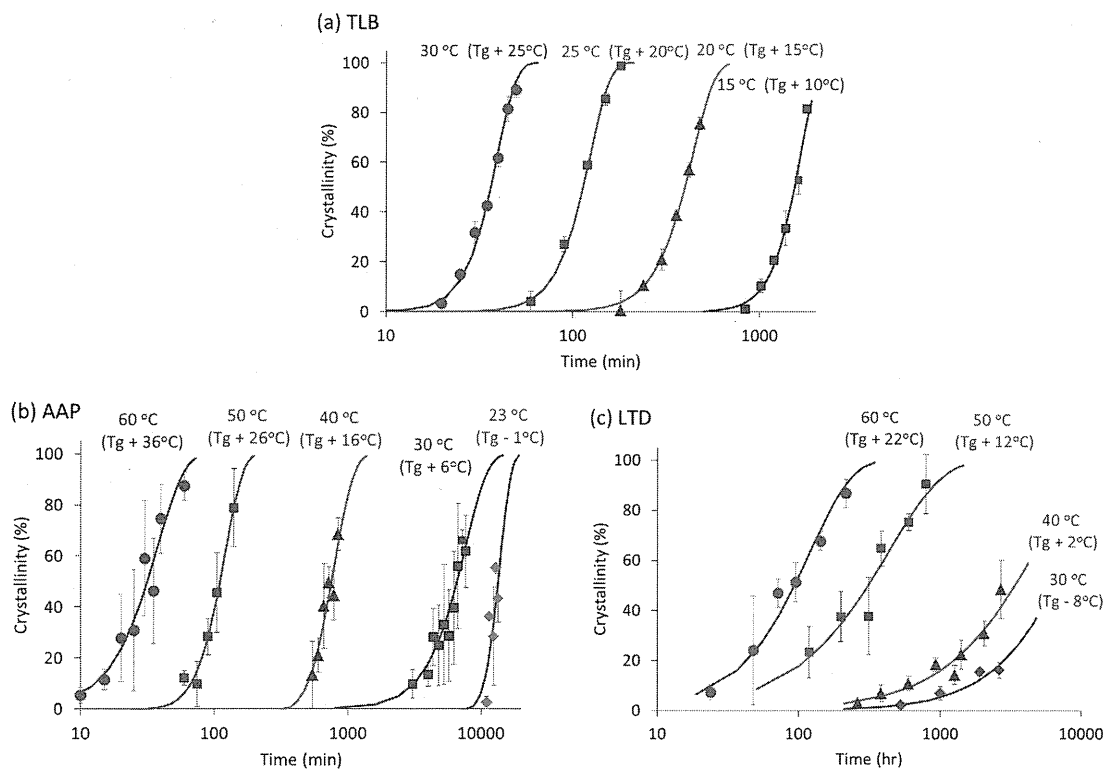
Figure 4. Evolution of crystallinity of the quenched TLB, AAP, and LTD as a function of time at the indicated temperature. The annealing was made either in DSC ($\leq$24 h) or temperature-controlled ovens (>24 h). Consistency of the two annealing procedures was confirmed for some samples. Each measurement was at least triplicated for showing error bars as standard deviations. The fitting lines were drawn based on the Avrami–Erofeev equation.

300 The crystallinity of chlorpropamide (CPA) and AAP
301 (crystallization to form III) was calculated by the same
302 procedure with that for TLB. Although NDP crystallized in
303 the same manner during heating, an exothermic transformation
304 peak just after the crystallization inhibited integration of the
305 peak because of their overlap. Thus, a shift in the baseline due
306 to partial crystallization was used to estimate the crystallinity,
307 which can be described by the following equation.

308 $$X(\%) = 100(W - W_\mathrm{a})/\Delta W \qquad (2)$$

309 where W and W_a are the heat flows of the annealed sample and
310 amorphous reference, which were obtained by cooling and
311 subsequent reheating after measurement of the annealed
312 sample. This equation is based on the fact that the crystalline
313 and amorphous states have their own heat capacities which
314 allow for determination of crystallinity by measuring the heat
315 capacity of the sample of interest. Due to the partial
316 crystallization, the heat capacity of the annealed sample was
317 between the heat capacities of crystalline and amorphous
318 samples, depending on the crystallinity. Because W and W_a are
319 functions of temperature, the values were read at the parallel
320 part of the heating curves between T_g and the crystallization
321 temperature, typically at 60 °C in the case of NDP. ΔW is the
322 difference in the heat flow between amorphous and crystalline
323 samples, for which the value of 0.0785 W/g was applied.
324 Theoretically, this method should be applicable to any
325 compounds and was confirmed to provide the same crystallinity
326 values for TLB and AAP. However, measurement of the correct
327 heat capacity requires very good thermal contact of the sample

with the bottom of the DSC pan.[18] The samples used in this 328
study met this requirement because they were prepared by 329
melt–quenching; however, it is not recommended to apply this 330
method to powder samples because of their poor thermal 331
contact. 332
The crystallinity for RTV and LTD was calculated from the 333
melting enthalpy because crystallization did not occur during 334
the heating process. Figure 3 shows DSC curves of the 335 f3
annealed RTV samples at 60 °C and intact crystal (form II). 336
The RTV glass crystallized to form IV initially, followed by 337
transformation to form I after annealing for 7 days. 338
Crystallization to form IV was analyzed in this study. Some 339
samples were still in form IV even after 7 days; however, those 340
samples were excluded from the analysis because inclusion of 341
that data would result in a focus on the slow-crystallization 342
samples. The same crystallization/transformation pattern was 343
observed for samples annealed at 50 °C, where the trans- 344
formation was initiated after annealing for 70 days. Although we 345
did not observe this transformation at 45 °C at least for 9 346
months, it is expected that after sufficiently long storage it will 347
occur because forms I and IV are monotropically related. The 348
crystallinity, X, was calculated using the following equation. 349

$$X(\%) = 100\left(\frac{H_\mathrm{m}}{H_\mathrm{mi}}\right)\left(\frac{H_\mathrm{m\text{-}II}}{H_\mathrm{m\text{-}IV}}\right) \qquad (3)$$ 350

where H_m, H_mi, $H_\mathrm{m\text{-}II}$, and $H_\mathrm{m\text{-}IV}$ are the melting enthalpies of 351
the annealed sample, the sample before the quenching, form II 352
(87.8 J/g), and form IV (59.8 J/g),[20] respectively. 353

354 LTD crystallized to a stable form below 30 °C (T_m = 135
355 °C), while it crystallized to the metastable form above 50 °C
356 (T_m = 133 °C).

357 **Analysis of the Crystallization Process.** Figure 4 shows
358 crystallization curves of model compounds annealed under
359 various temperature conditions. Each data set was fitted using
360 the Avrami—Erofeev equation as shown below.

$$361 \quad X(\%) = 100[1 - \exp\{-k(t - d)^n\}] \qquad (4)$$

362 where k and d are the crystallization rate constant and
363 induction time, respectively. n is an Avrami exponent, which is
364 determined by the dimension of the crystal growth and
365 nucleation mechanism. TLB exhibited very high reproducibility
366 in its crystallization behavior, as demonstrated by the small
367 error bars for each data point; this is presumably because
368 crystallization is basically governed by thermodynamics. The
369 same trend was observed for another class I compound, CPA.
370 AAP and NDP are class II compounds, and RTV and LTD are
371 class III compounds. Obviously, reproducibility of each point
372 was lower than those for class I compounds.

373 Figure 5 shows the time when crystallinity reached 10%, t_{10},
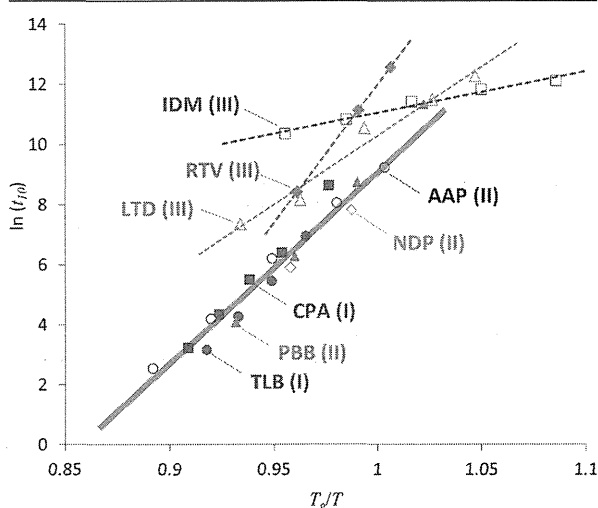374 as a function of the reduced temperature, T_g/T. In this figure,

Figure 5. 10% crystallization time (initiation time, in the unit of min)
as a function of T_g/T for all the model compounds. Symbols: TLB
(●), CPA (■), AAP (O), NDP (◇), LTD (△), RTV (◆). Literature
data for indomethacin (IDM, □)[21] and phenobarbital (PBB, ▲)[9] is
also presented. The fitting line ("general line") was drawn for TLB,
CPA, AAP, NDP, and PBB, which showed temperature-dominated
crystallization (i.e., thermodynamically controlled compounds) and
can be expressed by $\ln(t_{10}) = 66.2(T_g/T) - 57.0$.

375 the literature data for indomethacin (IDM)[21] and phenobarbi-
376 tal (PBB)[9] is also presented. Hereafter, t_{10} is referred to as the
377 initiation time. Note that the induction time, d, is a more
378 reasonable parameter for describing timing when crystallization
379 begins; however, the reliability of d obtained from Avrami
380 fitting is generally poor because of shape of logarithmic
381 function.[22] In contrast, reliability of t_{10} value is much higher and
382 its validity can easily be judged from interpolation of the raw
383 data around 10% crystallinity. Even for cases where the
384 crystallization is very slow, t_{10} can be obtained without
385 performing experiments over a long period, while the entire
386 crystallization curve is required for obtaining d from the Avrami

387 fitting. Thus, t_{10} is a practical parameter to evaluate the time
388 when crystallization begins.

389 The most important finding in Figure 5 is that the data for
390 classes I (TLB, CPA) and II (AAP, NDP, PBB) compounds fell
391 on the same line at least above T_g. Thus, if crystallization of the
392 compounds is governed by thermodynamics to some extent,
393 their initiation time can be described as a function of only T_g.
394 The line passes through approximately $\ln(t_{10}) = 9$ at $T_g/T = 1$,
395 meaning that any class I and II compounds should start to
396 crystallize in 6 days at T_g. Although this value has a deviation of
397 approximately one order, there is demonstrable universality in
398 the initiation time regardless of the compound species. The
399 slope of the universal line provides the ratio of activation energy
400 (E_a) for initiating crystallization to T_g as ca. 550 J/(mol·K), and
401 from this value, E_a could be calculated as 217, 221, 243, and 245
402 kJ/mol, respectively, for CPA, TLB, AAP, and NDP. Thus, E_a
403 roughly correlates with the crystallization tendency (energetic
404 barrier for crystallization) during the cooling/heating cycle in
405 DSC, but the differences are not significant.

406 The initiation time for class III compounds (LTD, RTV,
407 IDM) was significantly longer than for class I and II
408 compounds, i.e., the thermodynamically controlled compounds.
409 The poor reproducibility in the crystallization behavior of these
410 compounds indicated that stochastic nucleation plays an
411 important role in determining the initiation time.

Relevance of Nucleation Mechanism to the Dominant
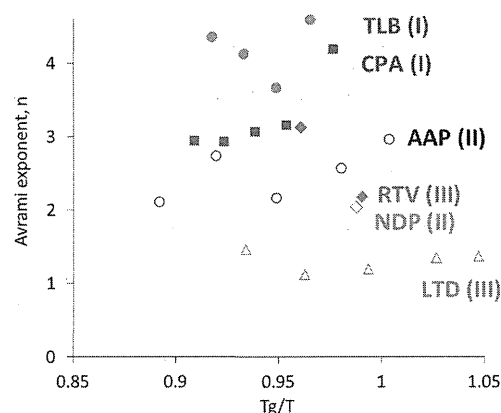**Factor for Crystallization.** Figure 6 shows the Avrami

Figure 6. Avrami exponents as a function of T_g/T for all the model
compounds, which were obtained by the fitting to the Avrami—Erofeev
equation as shown in Figure 4. Symbols are the same as those for
Figure 5

414 exponent obtained by fitting the Avrami—Erofeev equation.
415 The Avrami exponent, which depends on the nucleation
416 mechanism and dimensions of the crystal growth, generally
417 exhibited a large value for class I compounds, followed by class
418 II and III compounds. The value for TLB was constant at ca. 4,
419 which can only be understood by three-dimensional crystal
420 growth after homogeneous nucleation. It is most likely that
421 compounds of lower classes tend to nucleate homogeneously,
422 and with higher classes, the nucleation mechanism changes to
423 heterogeneous.

424 Synchrotron WAXD and DSC simultaneous measurements
425 were applied for observing crystallization of TLB and AAP.
426 Figure 7 shows two-dimensional WAXD after crystallization.
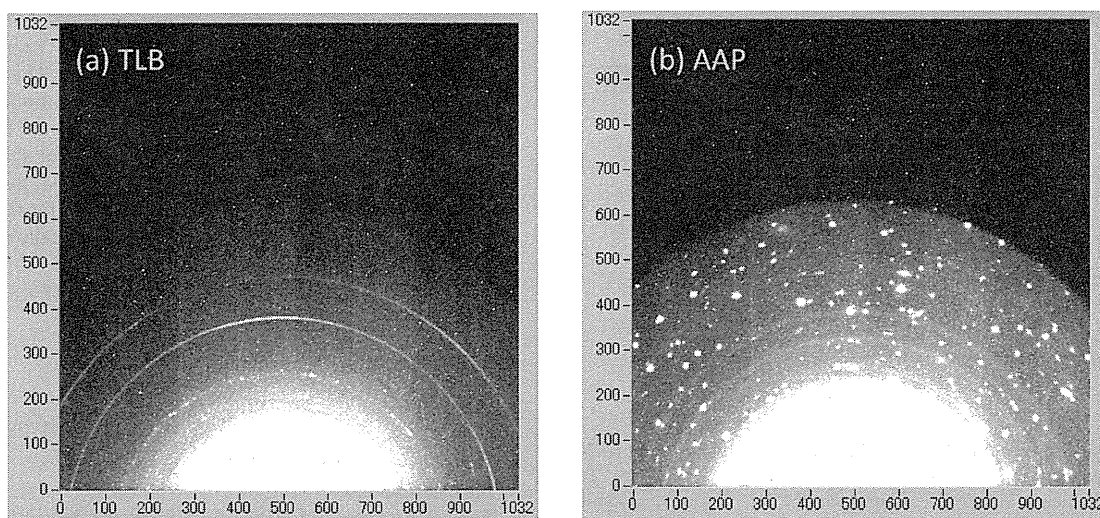427 TLB produced a diffraction ring pattern, indicating that small

Figure 7. X-ray diffraction rings obtained for TLB and APP using synchrotron radiation source, which were crystallized during cooling at 5 °C/min and reheating at 5 °C/min, respectively.

428 nuclei were formed immediately, but the size of the grown
429 crystals was small. In contrast, a few nuclei should have been
430 produced for AAP, leading to the formation of large single
431 crystals because many diffraction spots were obtained in
432 WAXD. This result supports the assumption of the nucleation
433 mechanism based on the Avrami exponents. The thermody-
434 namically controlled crystallization of class I compounds seems
435 to be closely related to their nucleation mechanism, which is
436 homogeneous nucleation. In contrast, the kinetic factor seems
437 to play a partial role in the crystallization behavior if the
438 nucleation is heterogeneous.
439   A similar observation on the relationship of the crystallization
440 rate, nucleation mechanism, and Avrami exponent was
441 previously made on the pharmaceutical ester oil, Imwitor
442 742.[23] It crystallized to the form α immediately upon cooling
443 below −20 °C, while a temperature-dependent slow crystal-
444 lization to form β was observed above this temperature. The
445 microscopic observation indicated that the crystallization to the
446 forms α and β seemed be initiated by homogeneous and
447 heterogeneous nucleation, respectively. The Avrami exponent
448 was only available for the form β, and it also supported the
449 connection between slow crystallization and heterogeneous
450 nucleation. Furthermore, poor reproducibility in the induction
451 time for crystallization of the form β indicated that stochastic
452 nucleation played an important role in the case of the
453 heterogeneous nucleation.
454   Figure 8 shows the crystallization rate as a function of
455 reduced temperature. The compounds of the lower class
456 exhibited a steeper slope. In addition to the temperature
457 dependence of the crystallization rate itself, variation in the
458 initiation time influenced the calculation because it made the
459 time required for crystallization apparently longer. If crystal-
460 lization of each sample is analyzed individually, the
461 crystallization rate should be smaller. Such analysis was
462 performed in our previous study, using Imwitor to find that
463 the crystallization rate was not sensitive to temperature in the
464 temperature range, where a long initiation time is required.
465   **Quantitative Prediction of Storage Stability.** If a trace
466 amount of crystals exists in the amorphous formulation, it
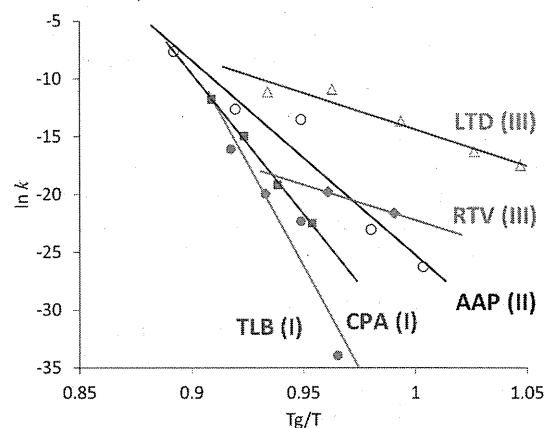467 significantly enhances crystallization after dispersion to the

Figure 8. The crystallization rate as a function of reciprocal time. Symbols are the same as those for Figure 5

medium. The presence of 10% crystal would be sufficient to 468
impair the advantage of amorphous dosage forms. Thus, the 469
most important parameter to be predicted in the developmental 470
study is the initiation time despite a wide variation in the 471
crystallization rate after nucleation. Figure 9 shows the 472 f9
initiation time of the crystallization as a function of T_g for 473
compounds in which crystallization is basically governed by 474
thermodynamics (classes I and II). If a three-year stability is 475
desired, T_g must be higher than 48 or 26 °C for storage at 25 or 476
5 °C, respectively. The differences between the critical T_g and 477
storage temperature are 23 and 21 °C, respectively. Class III 478
compounds should be more stable; however, a sufficient 479
stability margin must be considered because of the poor 480
reproducibility in the crystallization behavior. The initiation 481
time for thermodynamically controlled compounds may be 482
regarded as the worst case for class III compounds. In 483
conclusion, the "shortest" initiation time for any compound can 484
be generalized by the universal line shown in Figure 5, which 485
provides more optimistic criteria than the T_g −50 °C rule.[2] It 486
should be noted that the "general line" in Figure 5 was basically 487
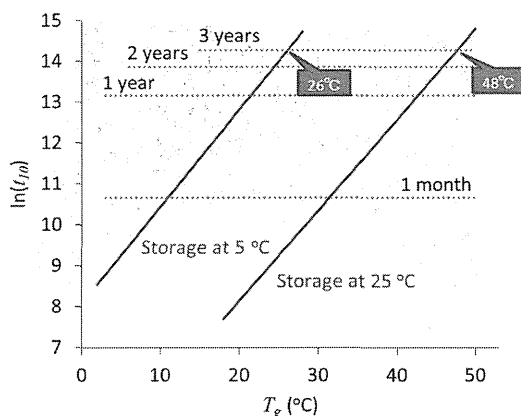
Figure 9. Initiation time of the thermodynamically controlled crystallization as a function of the glass transition temperature. The general line in Figure 5 was used for the calculation by assuming storage at 5 or 25 °C.

drawn using the data above T_g. Validity of its extrapolation to the lower temperature requires further investigation.

The formulation stability should be much better than that of the amorphous drug. In this paper, only the stability of the drug molecule is discussed which can be regarded as the worst case for formulation stability. It is also expected to be predicted from the mixture T_g; however, much care is required for miscibility in multicomponent systems. Although molecular-level mixing between drug and excipient molecules is expected for amorphous formulations, current analysis techniques only allow for investigation of miscibility on larger scales. For example, DSC is usually investigating miscibility on a 10–100 nm scale.[24] Although solid-state nuclear magnetic resonance can evaluate smaller scale miscibility, the lower limit is a few nanometers.[24] Moreover, miscibility can change during storage and even during measurements.[25] If molecular clusters of drug molecules, of which the size may be below nano-order, exist in the formulation, the formulation stability may almost be equal to drug stability, which can be predicted as presented in this study.

The surface area of the melts was minimized and their contact with moisture was shielded in this study. If the formulation is prepared by hot-melt extrusion without applying subsequent milling, a similar level of stability may be achieved. However, powder formulations will have a lower stability than those of the melts because crystallization is frequently initiated at the surface.[26–28] Further studies that consider the effect of surface area and contact with moisture must be performed to establish a more general idea for predicting the physical stability of practical amorphous formulations.

■ CONCLUSIONS

Crystallization behaviors of pharmaceutical glasses which have wide variation in crystallization tendency during cooling from the melt have been investigated. The classification system proposed by Taylor et al. was employed for evaluating relative contributions of thermodynamic and kinetic factors in the crystallization process. The class I compounds, for which the thermodynamic factor (temperature) plays a dominant role, exhibited high reproducibility in the crystallization rate, probably due to their homogeneous nucleation. Crystallization of the class II compounds was also essentially governed by

thermodynamics; however, the nucleation might be heterogeneous, which led to lower reproducibility in crystallization behavior than that for the class I compounds. The initiation time for crystallization of class I and II compounds had universal activation energy, ca. 210–250 kJ/mol, and thus could be generalized as a function of only T_g/T. As for the class III compounds, the crystallization appeared to be initiated by stochastic nucleation. Better stability is expected for the class III compounds, although reproducibility in crystallization was lower than for the class I and II compounds. This analysis should make the physical stability of pharmaceutical glasses predictable.

■ AUTHOR INFORMATION

Corresponding Author
*Phone: +81-29-860-4424. Fax: +81-29-860-4708. E-mail: kawakami.kohsaku@nims.go.jp.

Present Address
⊥For E.Y.: Institute of Medicinal Chemistry, Hoshi University, 2-4-41 Ebara, Shinagawa, Tokyo 142–8501, Japan.

Notes
The authors declare no competing financial interest.

■ REFERENCES

(1) Serajuddin, A. T. M. Solid Dispersion of Poorly Water-Soluble Drugs: Early Promises, Subsequent Problems, and Recent Breakthroughs. *J. Pharm. Sci.* **1999**, *88*, 1058–1066.

(2) Yu, L. Amorphous Pharmaceutical Solids: Preparation, Characterization and Stabilization. *Adv. Drug. Delivery Rev.* **2001**, *48*, 27–42.

(3) Kawakami, K. Current Status of Amorphous Formulation and Other Special Dosage Forms as Formulations for Early Clinical Phases. *J. Pharm. Sci.* **2009**, *98*, 2875–2885.

(4) Kawakami, K. Modification of Physicochemical Characteristics of Active Pharmaceutical Ingredients and Application of Supersaturatable Dosage Forms for Improving Bioavailability of Poorly Absorbed Drugs. *Adv. Drug Delivery Rev.* **2012**, *64*, 480–495.

(5) Bhugra, C.; Pikal, M. J. Role of Thermodynamic, Molecular, and Kinetic Factors in Crystallization from the Amorphous State. *J. Pharm. Sci.* **2008**, *97*, 1329–1349.

(6) Miyazaki, T.; Yoshioka, S.; Aso, Y.; Kawanishi, T. Crystallization Rate of Amorphous Nifedipine Analogues Unrelated to the Glass Transition Temperature. *Int. J. Pharm.* **2007**, *336*, 191–195.

(7) Baird, J. A.; van Eerdenbrugh, B.; Taylor, L. S. A Classification System to Assess the Crystallization Tendency of Organic Molecules from Undercooled Melts. *J. Pharm. Sci.* **2010**, *99*, 3787–3806.

(8) Mahlin, D.; Ponnambalam, S.; Hockerfeit, M. H.; Bergstrom, C. A. S. Toward in Silico Prediction of Glass-Forming Ability from Molecular Structure Alone: A Screening Tool in Early Drug Development. *Mol. Pharmaceutics* **2011**, *8*, 498–506.

(9) Aso, Y.; Yoshioka, S.; Kojima, S. Relationship between the Crystallization Rates of Amorphous Nifedipine, Phenobarbital, and Flopropione, and Their Molecular Mobility as Measured by Their Enthalpy Relaxation and ¹H NMR Relaxation Times. *J. Pharm. Sci.* **2000**, *89*, 408–416.

(10) Kaminski, K.; Adrjanowicz, K.; Wojnarowska, Z.; Dulski, M.; Wrzalik, R.; Paluch, M.; Kaminska, E.; Kasprzycka, A. Do Intermolecular Interactions Control Crystallization Abilities of Glass-Forming Liquids? *J. Phys. Chem. B* **2011**, *115*, 11537−11547.

(11) Angell, C. A. Relaxation in Liquids, Polymers and Plastic Crystals—Strong/Fragile Patterns and Problems. *J. Non-Cryst. Solids* **1991**, *131–133*, 13−31.

(12) Crowley, K. J.; Zografi, G. The Use of Thermal Methods for Predicting Glass-Former Ability. *Thermochim. Acta* **2001**, *380*, 79−93.

(13) Senkov, O. N. Correlation between Fragility and Glass-Forming Ability of Metallic Alloys. *Phys. Rev. B* **2007**, *76*, 104202.

(14) Suryanarayana, C.; Seki, I.; Inoue, A. A Critical Analysis of the Glass-Forming Ability of Alloys. *J. Non-Cryst. Solids* **2009**, *355*, 355−360.

(15) Ping, W.; Paraska, D.; Baker, R.; Harrowell, P.; Angell, C. A. Molecular Engineering of the Glass Transition: Glass-Forming Ability across a Homologous Series of Cyclic Stilbenes. *J. Phys. Chem. B* **2011**, *115*, 4696−4702.

(16) Kawakami, K.; Pikal, M. J. Calorimetric Investigation of the Structural Relaxation of Amorphous Materials: Evaluating Validity of the Methodologies. *J. Pharm. Sci.* **2005**, *94*, 948−965.

(17) Adjanowicz, A.; Grzybowski, A.; Kaminski, K.; Paluch, M. Temperature and Volume Effect on the Molecular Dynamics of Supercooled Ibuprofen at Ambient and Elevated Pressure. *Mol. Pharmaceutics* **2011**, *8*, 1975−1979.

(18) Harada, T.; Kawakami, K.; Yoshihashi, Y.; Yonemochi, E.; Terada, K.; Moriyama, H. Practical Approach for Measuring Heat Capacity of Pharmaceutical Crystals/Glasses by Modulated-Temperature DSC. *Chem. Pharm. Bull.* **2013**, *61*, 315−319.

(19) Kawakami, K.; Usui, T.; Hattori, M. Understanding the Glass-Forming Ability of Active Pharmaceutical Ingredients for Designing Supersaturating Dosage Forms. *J. Pharm. Sci.* **2012**, *101*, 3239−3248.

(20) Morissette, S. L.; Soukasene, S.; Levinson, D.; Cima, M. J.; Almarsson, O. Elucidation of Crystal Form Diversity of the HIV Protease Inhibitor Ritonavir by High-Throughput Crystallization. *Proc. Natl. Acad. Sci. U. S. A.* **2003**, *100*, 2180−2184.

(21) Andronis, V.; Zografi, G. Crystal Nucleation and Growth of Indomethacin Polymorphs from the Amorphous State. *J. Non-Cryst. Solids* **2000**, *271*, 236−248.

(22) Avramov, I.; Avramova, K.; Russel, C. New Method to Analyze Data on Overall Crystallization Kinetics. *J. Cryst. Des.* **2005**, *285*, 394−399.

(23) Kawakami, K. Isothermal Crystallization of Imwitor 742 from Supercooled Liquid State. *Pharm. Res.* **2007**, *24*, 738−747.

(24) Kawakami, K.; Hasegawa, Y.; Deguchi, K.; Ohki, S.; Shimizu, T.; Yoshihashi, Y.; Yonemochi, E.; Terada, K. Competition of Thermodynamic and Dynamic Factors During Formation of Multicomponent Particles via Spray Drying. *J. Pharm. Sci.* **2013**, *102*, 518−529.

(25) Kawakami, K. Miscibility Analysis of Particulate Solid Dispersions Prepared by Electrospray Deposition. *Int. J. Pharm.* **2012**, *433*, 71−78.

(26) Crowley, K. J.; Zografi, G. The Effect of Low Concentrations of Molecularly Dispersed Poly(vinylpyrrolidone) on Indomethacin Crystallization from the Amorphous State. *Pharm. Res.* **2003**, *20*, 1417−1422.

(27) Wu, T.; Yu, L. Surface Crystallization of Indomethacin below T_g. *Pharm. Res.* **2006**, *23*, 2350−2355.

(28) Kawakami, K.; Zhang, S.; Chauhan, R. S.; Ishizuka, N.; Yamamoto, M.; Masaoka, Y.; Kataoka, M.; Yamashita, S.; Sakuma, S. Preparation of Fenofibrate Solid Dispersion Using Electrospray Deposition and Improvement in Oral Absorption by Instantaneous Post-Heating of the Formulation. *Int. J. Pharm.* **2013**, *450*, 123−128.

Research Article

Simultaneous Determination of Polyethylene Glycol-Conjugated Liposome Components by Using Reversed-Phase High-Performance Liquid Chromatography with UV and Evaporative Light Scattering Detection

Hiroko Shibata,[1,2] Chikako Yomota,[1] and Haruhiro Okuda[1]

Abstract. Liposomes incorporating polyethylene glycol (PEG)-conjugated lipids (PEGylated liposomes) have attracted attention as drug delivery carriers because they show good *in vivo* stability. The lipid component of PEGylated liposomal formulations needs to be quantified for quality control. In this study, a simple reversed-phase high-performance liquid chromatography (HPLC) method with an evaporative light-scattering detector (ELSD) was established for simultaneous determination of hydrogenated soy phosphatidylcholine, cholesterol, PEG-conjugated lipid, and hydrolysis products of phospholipid in PEGylated liposomal formulations. These lipids were separated using a C18 column with a gradient mobile phase consisting of ammonium acetate buffer and ammonium acetate in methanol at a flow rate of 1.0 ml/min. This method provided sufficient repeatability, linearity, and recovery rate for all lipids. However, the linearity and recovery rates of cholesterol achieved using a ultraviolet (UV) detector were better than those achieved using an ELSD. This validated method can be applied to assess the composition change during the preparation process of liposomes and to quantify lipid components and hydrolysis products contained in a commercially available liposomal formulation DOXIL®. Taken together, this reversed-phase HPLC-UV/ELSD method may be useful for the rapid or routine analysis of liposomal lipid components in process development and quality control.

KEYWORDS: component analysis; evaporative light scattering; liposome; reversed-phase HPLC.

INTRODUCTION

Liposomes, which are closed vesicles consisting of a lipid bilayer, have been studied as drug delivery carriers, and have been applied in clinical treatments. It is well known that liposomes incorporating polyethylene glycol (PEG)-conjugated lipid (PEGylated liposomes) can escape uptake by the reticuloendothelial system (RES) and circulate in the blood stream for a prolonged period of time (1,2). Moreover, PEGylated liposomal doxorubicin—DOXIL®—has been marketed and is available commercially. Ambisome®, which contains amphotericin B in the lipid bilayer, demonstrates properties that tend to be uptaken by RES because of anionic lipids in the bilayer and exhibits anti-fungal effects within the RES (3). In gene delivery, cationic liposomes are widely used and numerous attempts have been made to increase the gene transfection efficiency by using ligand-modifying and functional lipids (4). Thus, the "liposome" does not exist, and the lipid component of liposomes is dependent on the encapsulated drug or the objective product performance. Therefore, the lipid and polymeric modifier composition is one of the important physicochemical properties to ensure the quality/safety/efficacy of liposomal products.

Hydrolysis is the primary chemical degradation process of phospholipids. The hydrolysis of ester functionalities is unavoidable in the presence of water, which results in the production of lysophospholipids and free fatty acids. Lysophospholipids may also be further degraded into glycerophosphorylcholine and free fatty acids. It has been reported that increased concentrations of degradation products in liposomal formulations enhance permeability and cause destabilization of the lipid bilayer (5), which significantly affects particle size and can change the structure of the lipid assembly from lamellar to micellar (6). Thus, lipid hydrolysis is considered a critical parameter for the chemical stability of liposomal products. A considerable amount of research has been conducted on the factors that affect the hydrolysis rate, including pH and ionic strength of the storage solution (7–9). Because of these factors, the "assay of lipid components" and "degradation products related to the lipids" are recommended for pharmaceutical specifications in the draft guidance presented by the US FDA for liposomal products (10). This guidance also recommends the development of a stability test which would help evaluate the chemical stability of lipids in liposomal formulations as well as the stability of the

encapsulated drug, by measuring degradation products such as lysophospholipids and free fatty acids. Thus, appropriate methods for the quantification of lysophospholipids and free fatty acids as well as the liposomal components are required to ensure the efficacy and safety of liposomal products.

High-performance liquid chromatography (HPLC) is widely used to separate and analyze lipids of various origins into lipid classes or molecular species. While unsaturated lipids may be analyzed by ultraviolet (UV) detection, saturated lipids, which are commonly used in liposomal formulations, have no specific absorbance in the UV region, and conventional UV detection cannot be used unless derivatized. Thus, the refractive index detector (RID), evaporative light-scattering detector (ELSD), charged aerosol detector (CAD), and MS were applied for the simultaneous HPLC analysis of lipids (8,11–13). Since ELSDs are higher sensitivity than that exhibited by RIDs, compatible with gradient elution, more easily available than CAD, and simpler to maintain than LC-MS, they are widely used for lipid analyses. Several HPLC-ELSD methods for the analysis of lipids or the hydrolysis products of phospholipids have been previously reported; however, the normal-phase separation was often used, which resulted in the large consumption of chloroform (14–17). While the reversed-phase separation method for the analysis of lipids in cationic liposomes have been reported (18), the reversed-phase separation methods for the simultaneous analysis of PEG-conjugated lipid and the hydrolysis products in PEGylated liposomes have not been well studied. Thus, in this study, we attempted to develop a reversed-phase HPLC-ELSD system that could simultaneously analyze the lipid components and hydrolysis products in PEGylated liposomes.

MATERIALS AND METHODS

Materials and Buffer Solutions

Hydrogenated soy phosphatidylcholine (HSPC; C16:0, 11.4% and C18:0, 88.6%) and N-(carbonyl-methoxy polyethyleneglycol 2000)-1,2-distearoyl-sn-glycero-3-phosphoethanolamine (DSPE-PEG), 1-palmitoyl-2-lyso-sn-glycero-3-phosphocholine (P-LysoPC), and 1-stearoyl-2-lyso-sn-glycero-3-phosphocholine (S-LysoPC) were purchased from Nippon Oil and Fat (Tokyo, Japan). Analytical-grade cholesterol (Chol), palmitic acid (PA), stearic acid (SA), HPLC-grade methanol, and ammonium acetate were purchased from Wako Pure Chemical (Osaka, Japan). Trifluoroacetic acid (TFA) was from Sigma-Aldrich Co (MO). Four lots (#011AFL, 012AGD, 029BJD, and 032BKA) of DOXIL® (JANSSEN PHARMACEUTICAL K.K, Tokyo, Japan) were purchased from a general sales agency for drugs, and the approximate elapsed time of each lot after manufacture was 68, 65, 29, and 26 months, respectively.

Standard stock solutions of PA, SA, P-LysoPC, S-LysoPC, HSPC, Chol, and DSPE-PEG were individually prepared by dissolving 3.0 mg of each lipid in 10 ml of methanol and stored at 4°C. The calibration standards were then prepared by diluting the standard stock solutions with methanol.

Instrumentation and Chromatographic Conditions

The apparatus used for the HPLC system consisted of two constant pumps (LC-10ADvp, Shimadzu, Kyoto, Japan),

a degasser (DGU-14A, Shimadzu), an automated pretreatment system, an autoinjector (SIL-10ADvp, Shimadzu), a column oven (CTO-10ACvp, Shimadzu), a UV detector (SPC-20AV, Shimadzu), an ELSD (ELSD-LTII, Shimadzu), and a system controller (SCL-10Asp, Shimadzu). A nitrogen generator (SLP-221ED, ANEST IWATA, Yokohama, Japan) was used as the source for the nitrogen gas. Data analysis was performed with the LC Solution program (Shimadzu). The separation was performed at 45°C on a YMC-Triart C18 column (150×4.6 mm i.d., 5 μm) from the YMC Co. (Kyoto, Japan). The ELSD conditions were as follows: the drift tube temperature was set at 45°C, the nitrogen gas-pressure was set at 350 kPa, and the gain was set to 6. The flow rate was 1.0 ml/min for the mobile phases (mobile phase A, 4 mM ammonium acetate buffer (pH 4.0) and mobile phase B, 4 mM ammonium acetate in methanol). The binary linear gradient began from a mixture of 20% A and 80% B and ended at 100% B in 10 min. After the 10-min plateau at 100% B, the mobile phase composition changed back to its initial composition in 5 min. The liposome samples were directly diluted with methanol to the lipid concentration within the calibration range. DOXIL® was diluted 10- or 20-fold, and the liposomes under the preparation were 10-fold diluted. The sample injection volume was 20 μl.

Liposomal Preparation

The lipid composition of PEGylated liposome referred to DOXIL®. The liposome, which consisted of HSPC/Chol/DSPE-PEG, was prepared using a modified ethanol injection method (19). Briefly, 47.9 mg of HSPC, 15.95 mg of Chol, and 15.95 mg of DSPE-PEG were dissolved in approximately 10 ml of ethanol. The ethanol was then removed using a rotary evaporator, which left behind approximately 1 ml of ethanol solution. Next, 8 ml of 10% sucrose (pH 6.5) was added to the ethanol solution. Liposomes formed spontaneously after further evaporation of the residual ethanol, and were extruded through a series of polycarbonate filters (Nucleopore, CA) with pore sizes ranging from 0.4 to 0.1 μm. Following the extrusion, the liposome solution was placed in membrane tubing with a molecular weight cut-off of 50 kDa (Flat-A-Lyzer G2, Spectrum Laboratories, Inc., CA) and was dialyzed against fresh 10% sucrose solution to remove the free lipids or micelles.

Incubation of Liposome

Each 500 μl of liposome in glass tubes were incubated at 37°C or 57°C in a water bath without agitation, or at 4°C in a refrigerator for three days. After incubation, liposomes were diluted 10-fold with methanol, and 20 μl of aliquots were injected to HPLC system.

RESULTS AND DISCUSSION

Optimization of the Separation Conditions

The method for the quantification of lipids in a laboratory preparation of liposomes as well as liposomal formulation development and quality control should be simple, rapid, and safe. Thus, we aimed to develop an HPLC-ELSD system that would quickly and simultaneously separate all of the
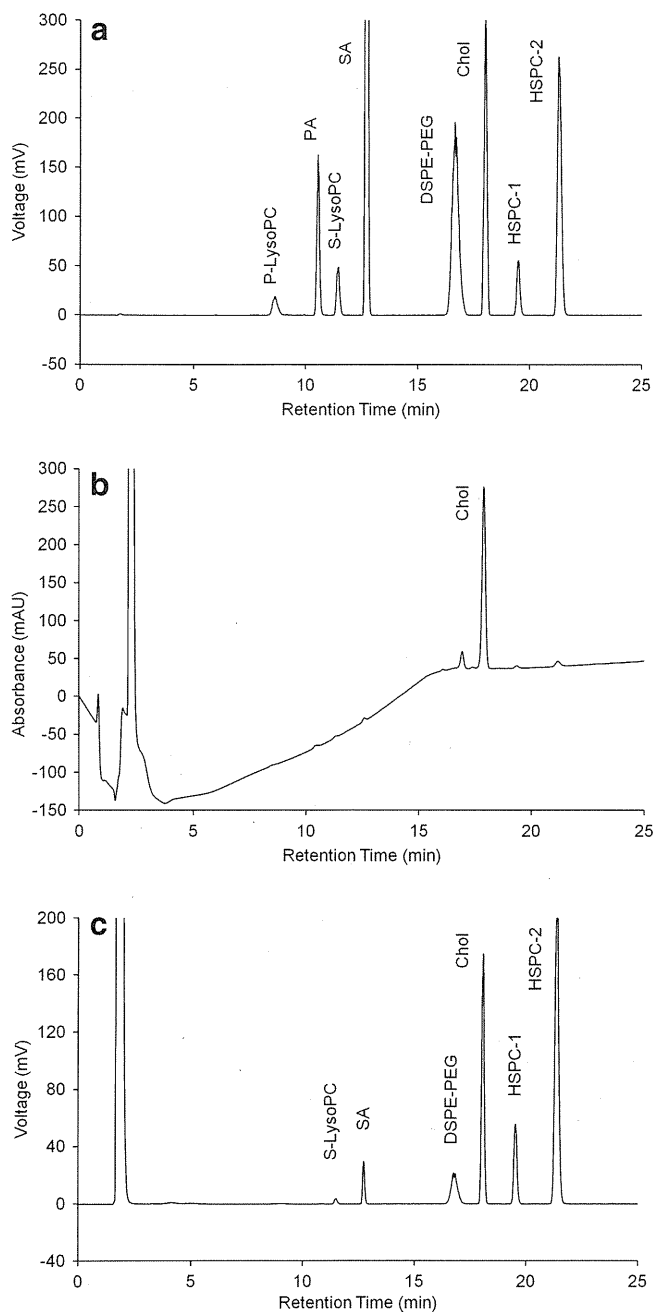
C18 column with TFA or ammonium acetate in methanol. However, the mobile phase with TFA did not provide a reproducible retention time for DSPE-PEG, and thus the mobile phase with ammonium acetate was selected. Using an isocratic elution with methanol-ammonium acetate buffer, a stable separation of lipid components, lysoforms, and fatty acids was obtained after optimization of the volume ratio, concentration, and pH of the ammonium acetate buffer (Figs. 1, 2, 3, and 4 in the Electronic Supplementary Materials). The HSPC, which consists of fatty acids, C16 and C18, showed two peaks, HSPC-1 and HSPC-2. Since PEG has a distribution of molecular weight, the peak shape of DSPE-PEG was broad. While there were no effects on the concentration of ammonium acetate (25–400 mM) on the Chol and HSPC, the higher concentration of ammonium acetate was associated with the faster retention time of DSPE-PEG. Although the details remain unclear, a large amount of ammonium ions may ionically interact with the anionic portion of the DSPE-PEG and increase its polarity.

The separation of the lipid components and hydrolysis products was possible using an isocratic mobile phase with methanol–200 mM ammonium acetate buffer (pH 4.0) (98:2, v/v). To clearly separate the lysoforms and fatty acids from the highly polar materials in the liposomal formulations, such as the active ingredient and sucrose, gradient elution was optimized. To maintain a steady level of ammonium acetate, 4 mM

Fig. 1. Comparison of the chromatograms detected by ELSD (a) and UV (b). A standard mixture (20 μl) containing 150 μg/ml (each) of P-LysoPC, S-LysoPC, PA, and SA; 300 μg/ml of Chol; and 750 μg/ml each of HSPC and DSPE-PEG was injected. The chromatogram of DOXIL® detected by ELSD (c). DOXIL® was diluted 10-fold with methanol, and 20-μl aliquots of the diluted solution were injected

lipids in the PEGylated liposomal formulations, which are not only liposomal lipids, but also the hydrolyzed products (lysophospholipids and free fatty acids). It has been reported that the hydrolysis of phosphatidylcholine predominantly produces 1-acyl-2-lyso-phosphatidylcholine with free fatty acids (8). Thus, 1-acyl-2-lysoforms were analyzed. Consistent with previous reports describing reversed-phase HPLC methods for lipids (18), the HPLC separation was optimized using a
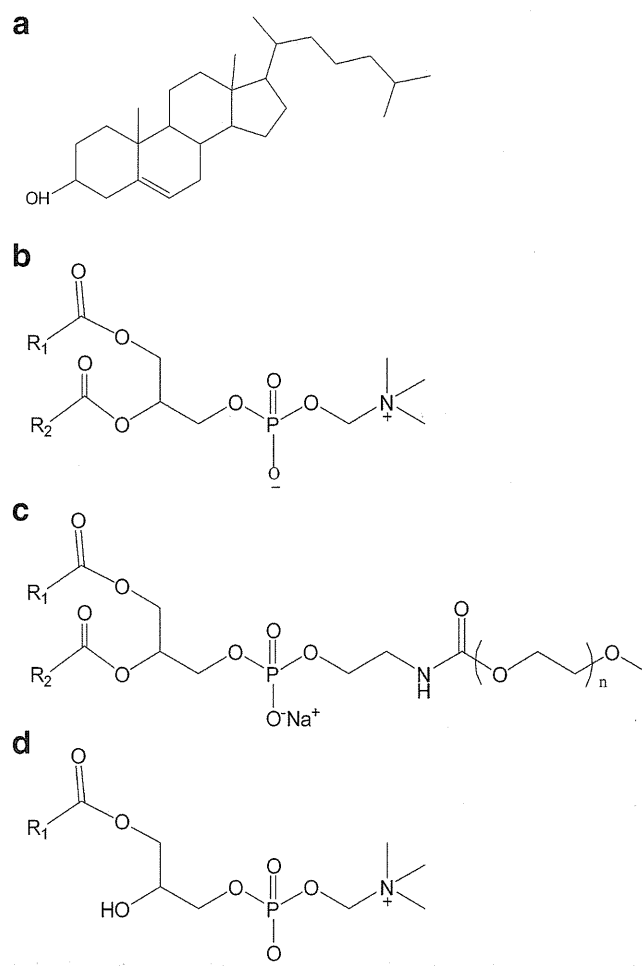

Fig. 2. Structure of a cholesterol, b HSPC, c DSPE-PEG, and d S-LysoPC)

Table I. Variability of Retention Times and Peak Areas of Standard Lipids ($n=6$), Limits of Detection (LOD), and Limits of Quantification (LOQ)

Lipid	Concentration (μg/ml)	Within-day Retention time (min, RSD)	Within-day Average area (mVs, RSD)	Between-day Retention time (min, RSD)	Between-day Average area (mVs, RSD)	LOD (μg/ml)	LOQ (μg/ml)
S-LysoPC	22.5	10.90 (0.33)	69.40 (3.62)	10.90 (0.13)	71.35 (4.20)	3.65	7.95
SA	12	12.33 (0.20)	316.22 (2.86)	12.33 (0.17)	334.65 (4.58)	1.31	2.36
DSPE-PEG	75	16.28 (0.16)	282.59 (1.68)	16.28 (0.08)	283.79 (1.55)	5.92	15.06
Chol	75	17.47 (0.06)	1,209.61 (2.81)	17.47 (0.05)	1,220.09 (2.64)	2.48	4.77
HSPC-1	240	18.75 (0.06)	267.60 (2.62)	18.76 (0.12)	257.80 (3.56)	12.42	34.35
HSPC-2	240	20.33 (0.07)	1,675.54 (2.41)	20.34 (0.13)	1,668.74 (2.95)	5.47	14.28

RSD relative standard deviation

ammonium acetate in methanol and 4 mM ammonium acetate buffer were used. The standard mixture which was diluted by methanol to obtain the target concentration was injected into the HPLC equipment, and sequentially monitored using a UV detector (205 nm) and the ELSD. A typical chromatogram is shown in Fig. 1a. Lipids were eluted in the order P-LysoPC, PA, S-LysoPC, SA, DSPE-PEG, Chol, HSPC-1, and HSPC-2 (Fig. 1a). Only the peak of the Chol was detectable using the UV detector; however, the other peaks could not be sufficiently obtained because of a lack of a C–C double bond (Fig. 1b). In contrast, higher and sharper peaks for all of the lipids were obtained using the ELSD (Fig. 1a). Next, to confirm the separation of the lipids from the additives in liposomal products, DOXIL® was diluted with methanol and injected into the HPLC equipment. A typical chromatogram is shown in Fig. 1c. Following the elution of highly polar materials such as doxorubicin and sucrose, the peaks of the hydrolysis products (S-LysoPC and SA) and lipid components in DOXIL® were obtained. Figure 2 shows the chemical structure of Chol and phospholipids detected in the sample of DOXIL®. Thus, the optimized analytical condition may be considered to exhibit sufficient sensitivity and separation for the quantification of lipid components and hydrolysis products in the liposomal products.

Method Validation

The developed HPLC-ELSD method for the analysis of lipids (S-LysoPC, SA, DSPE-PEG, Chol, HSPC-1, and HSPC-2) was validated with respect to repeatability, linearity, limits of detection (LOD) and quantification (LOQ), and accuracy (recovery rate). The within-day/between-day variability of the retention time and peak area of each lipid was evaluated (Table I). The between-day variability was determined on three different days by two different analysts. The relative standard deviation (RSD) values of the retention times were less than 0.33% for all lipids. For the peak areas, the RSD values using ELSD were higher. The LOD and LOQ for each lipid were evaluated (Table I). The LOD and LOQ values were calculated as three times the variation in the measured response (signal/noise ratio= 3) and ten times the variation (signal/noise=10), respectively. The values of the Chol and HSPC were the same number of digits as previously reported, which may be sufficient to determine the concentration of each lipid in the liposomal products.

Next, the linearity was tested for all lipids. Consistent with previous reports (20), the ELSD response was exponential rather than linear. The relationship between the peak area (A) and the concentration of each lipid (m) can be described as follows:

Table II. Standard Curves of Lipids in Methanol

Lipid		Regression equation	r^2
S-LysoPC (9.375–300 μg/ml)	Day 1	$y=98.049x^{1.6437}$	0.9985
	Day 2	$y=130.83x^{1.6063}$	0.9989
	Day 3	$y=124.16x^{1.6416}$	0.9988
SA (4.688–150 μg/ml)	Day 1	$y=493.39x^{1.9887}$	0.9992
	Day 2	$y=750.9x^{1.8791}$	0.9987
	Day 3	$y=525.74x^{2.027}$	0.9989
DSPE-PEG (18.75–600 μg/ml)	Day 1	$y=64.29x^{1.6745}$	0.9999
	Day 2	$y=64.848x^{1.6856}$	0.9999
	Day 3	$y=89.084x^{1.6294}$	0.9989
Chol (37.5–600 μg/ml)	Day 1	$y=5,759.3x^{1.0923}$	0.9957
	Day 2	$y=4,940.5x^{1.1139}$	0.9916
	Day 3	$y=4,722.9x^{1.1246}$	0.9950
HSPC-1 (46.875–1,500 μg/ml)	Day 1	$y=7.0282x^{1.7086}$	0.9995
	Day 2	$y=9.382x^{1.6658}$	0.9986
	Day 3	$y=9.2723x^{1.6605}$	0.9988
HSPC-2 (46.875–1,500 μg/ml)	Day 1	$y=31.233x^{1.7563}$	0.9980
	Day 2	$y=28.229x^{1.7698}$	0.9977
	Day 3	$y=21.056x^{1.8172}$	0.9973

Table III. The Recovery of the Lipid at Three Levels of Concentration: Accuracy of the HPLC-ELSD Method ($n=3$)

Lipid	Spiked concentration (μg/ml)	Recovered concentration (μg/ml)	Recovery (%)
S-LysoPC	15	15.02	100.10
	30	30.01	100.05
	60	58.57	97.62
SA	7.5	7.21	103.80
	15	14.76	98.42
	30	29.71	99.03
DSPE-PEG	75	74.77	99.69
	150	150.42	100.28
	300	302.67	100.89
Chol	75	85.38	113.83
	150	141.01	94.01
	300	285.06	95.02
HSPC-1	240	238.36	99.32
	480	468.95	98.59
	960	944.01	98.33
HSPC-2	240	238.99	99.58
	480	501.58	103.37
	960	964.63	100.48

$A=am^b$, where a and b are constants that are dependent on a variety of experimental conditions. A linear relationship was observed between the log (peak area) *versus* log (lipid concentration) for all lipids on three different days, where the correlation coefficients of S-LysoPC, SA, DSPE-PEG, HSPC-1, and HSPC-2 were greater than 0.997 (Table II). However, the correlation coefficient of Chol tended to be lower, from 0.9916 to 0.9957.

Recovery was assessed at low, medium, and high concentration levels of lipids. A stock standard solution for each lipid was diluted with methanol/10% sucrose (90/10, v/v) to obtain the theoretical concentration indicated in Table III, and three diluted solutions were individually injected. The average concentration was measured using the standard calibration curve of each lipid, and the average recovery rate was calculated based on the measured concentration against the theoretical concentration of each lipids. The recovery rates, except those for Chol, were 97.62–103.80%, indicating sufficient accuracy. The recovery rate of Chol was 94.01–113.83%, which did not suggest good accuracy. Because UV could sufficiently detect Chol as shown in Fig. 1, Chol was analyzed using the UV detector, which was placed in series with the ELSD, and the recovery rate for Chol was calculated (Table IV). The correlation coefficient for the calibration curve of Chol (*e.g.* $y=7,774.4x+46,171$) was 0.9999, and the recovery rate was 100.73–101.3%, indicating sufficient

Table IV. The Recovery Rate of Chol at Three Levels of Concentration: Accuracy of the HPLC-UV Method ($n=3$)

Lipid	Spiked concentration (μg/ml)	Recovered concentration (μg/ml)	RSD (%)	Recovery (%)
Chol	75	75.55	0.10	100.73
	150	151.94	0.10	101.30
	300	303.56	0.03	101.19

Table V. Effect of Processing Stage on Liposome Component ($n=3$)

Processing stage	Calculated lipid molar ratio (mean±SD; %)		
	Chol[a]	HSPC[b]	DSPE-PEG
Dissolved in ethanol	40.48±0.32	54.13±0.32	5.39±0.13
Evapolation	40.72±0.04	53.99±0.11	5.29±0.10
Particle size reduction	40.73±0.45	53.99±0.54	5.29±0.12
Dialysis	42.47±0.74	53.02±0.55	4.51±0.33

[a] Chol was detected by a UV detector
[b] The value of HSPC was calculated from the peak of HSPC-1

linearity and accuracy. These results indicated that the HPLC-ELSD method is applicable to the measurement of lipid components and hydrolysis products in liposomal formulation, while in the case of Chol, UV detection will be better using the same separation system. The low linearity of Chol, not additives in samples, can be considered a cause for the inadequate recovery rate because even the sample containing only Chol and methanol showed low recovery rate (data not shown). After an investigation, it was found that ammonium acetate in mobile phase affects the detection process of ELSD (droplet size/density/distribution by nebulization, and size/distribution of evaporated particles), and can cause a lower correlation coefficient between concentration and scattering intensity.

Application of the Method

A validated HPLC-UV/ELSD method was first used for the quantitative analysis of liposomes prepared in our laboratory. To quantify the HSPC, the main HSPC-1 peak was evaluated based on the linearity of both peaks. Adequate quantification of the prepared liposomes is critical to maintain the attributes (such as encapsulation efficiency and lipid composition rate) of the liposomal formulation. Moreover, the evaluation of changes in lipid composition will be needed to properly design the preparation (manufacturing) process. Changes in the lipid composition rate were assessed in the liposome preparation process (Table V). Compared with the lipid composition when lipids were dissolved in ethanol, there were no significant changes after the evaporation and particle size reduction. However, after the dialysis for external solution exchange, the percentages of HSPC and DSPE-PEG slightly decreased, whereas the percentage of Chol was slightly increased. The total lipid amount decreased by 5–10% following dialysis (data not shown). Thus, changes in the lipid component may be caused by the removal of HSPC and DSPE-PEG, which is not incorporated into the liposome, from the dispersing solution by dialysis.

Next, DOXIL® was quantified. Four product lots that were stored for a long period of time were compared. Two lots were stored for over 65 months and two lots were stored for 26–29 months (Table VI). Compared with the lipid composition described in the package insert of DOXIL®, the ratio of Chol was slightly higher, and the ratios of HSPC and DSPE-PEG were slightly lower. These slight differences may have been caused by the liposomal preparation process because the lipid composition described in the package insert was the quantity of